Role of Solvent on Nonenzymatic Peptide Bond Formation Mechanisms and Kinetic Isotope Effects

Katarzyna Świderek,[†,‡] Iñaki Tuñón,[*,‡] Sergio Martí,[§] Vicent Moliner,[*,§] and Juan Bertrán[∥]

[†]Institute of Applied Radiation Chemistry, Faculty of Chemistry, Lodz University of Technology, Zeromskiego 116, 90-924 Lodz, Poland

[‡]Departament de Química Física, Universitat de València, 46100 Burjassot, Spain

[§]Departament de Química Física i Analítica, Universitat Jaume I, 12071 Castelló, Spain

[∥]Departament de Química, Universitat Autònoma de Barcelona, 08193 Bellaterra, Spain

S *Supporting Information*

ABSTRACT: Based on the hypothesis that similar mechanisms are involved in the peptide bond formation in aqueous solution and in the ribosome, the aminolysis of esters in aqueous solution has been the subject of numerous studies as the reference reaction for the catalyzed process. The mechanisms proposed in the literature have been explored in the present paper by hybrid QM/MM molecular dynamics simulations. The free energy profiles have been computed with the QM region of the system described at semiempirical AM1 level and by DFT within the M06-2X functional. According to the results, the formation of adduct zwitterion species is a preliminary step required for all possible mechanisms. Then, from different conformers of this species, four different paths were found: three of them taking place through concerted mechanisms of four-, six- and eight-membered ring transition states, and a stepwise mechanism through a neutral intermediate. Comparison of the free energy profiles indicates that the concerted mechanisms would be kinetically favored, with free energy barriers in very good agreement with experimental data. Calculations of kinetic isotope effects, when including the solute interactions with the first solvation shell, show that the 8-membered ring TS renders values in better agreement with available experimental data. Quantitative discrepancies can be attributed to different employed models in experiments and calculations.
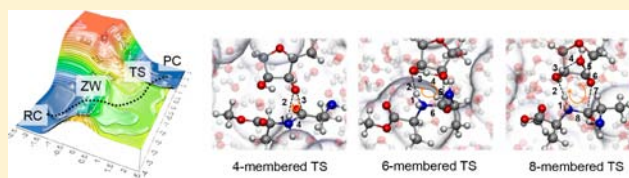
INTRODUCTION

Ribosomes are exquisitely complex molecular machines used by living organism to flow the genetic information encoded within genes into proteins. The ribosome catalyzes the peptide bond formation by the nuclephilic attack of an aminoacyl-tRNA in the A-site on peptidyl-tRNA in the P-site. Despite great progress in the study of ribosome function in the elongation step,[1−3] the mechanism of this process and the origin of the catalytic power of this ancient enzyme are still an unsolved puzzle. In this regard, many experimental and theoretical studies have focused on the aminolysis of esters in aqueous solution based on the hypothesis that similar mechanisms are involved in both media.[4−6]

Experimental studies based on liner free-energy relationships[7−12] and isotope substitution effects[13−18] in solution apparently support a stepwise mechanism with participation of different kind of intermediates, ranging from anionic, cationic, neutral, and zwitterionic species. Reactions of esters with aliphatic amines generally show breaks in their pH-rate profiles at pH 6.3−8.7, indicating a change in rate-limiting step and therefore the presence of intermediates.[19]

Computational studies have suggested the existence of basically three different mechanisms, as depicted in Scheme 1: (1) a concerted mechanism in which the nucleophilic attack on the amino group, the C−O cleavage bond, and the proton transfer take place simultaneously; (2) a stepwise mechanism through a neutral intermediate; and (3) a stepwise mechanism through a zwitterionic intermediate.[20−22] Mechanisms through positive or negative intermediates will not be explored, since our simulations are carried out at neutral pH, in the absence of additional bases or acids species.

The mechanism through the zwitterionic intermediate has been the subject of controversy since separated charges species cannot be located in gas phase or in solution by traditional continuum models.[20−24] The addition of a reduced number of explicit water molecules in the model has shown to be crucial to stabilize this intermediate,[24−26] as well as the use of the more recently developed solute electron density model (SMD)[27] that has shown to be capable of stabilizing zwitterionic species.[28] In this sense, Warshel and co-workers located a zwitterionic intermediate in the catalyzed methanolysis of formamide (formally the reverse reaction of the one studied in the present paper) by combined ab initio/Langevin dipoles calculations.[29] Thus, most of the theoretical studies have been focused on the first two mechanisms, the concerted and the stepwise

Scheme 1. Proposed Reaction Mechanism for the Aminolysis of Esters in Aqueous Solution[a]
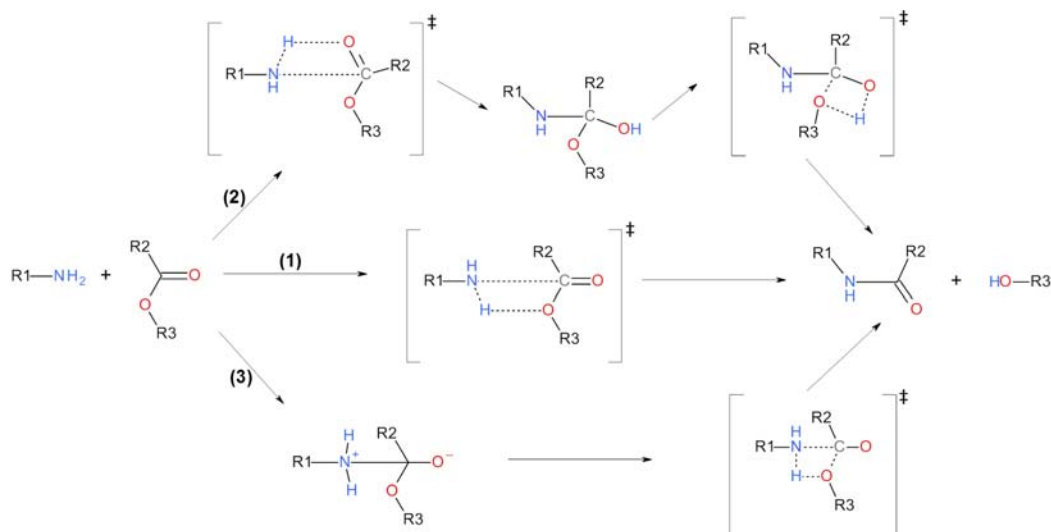
[a](1) Concerted mechanism, (2) stepwise mechanism through a neutral intermediate, and (3) stepwise mechanism through a zwitterionic intermediate.

mechanism involving a neutral intermediate.[20,22,23,30−33] Some studies have shown the catalytic activity of an additional molecule, water,[32,34] or ammonia,[20,22,33] by reducing the activation barrier. Also, the catalytic effect of vicinal hydroxyl groups, through hydrogen bond interactions or even stronger effects if a proton shuttle mechanism is allowed via hexagonal transition state, has been also shown.[35−37] It is important to point out that mentioned theoretical studies have been performed with simple models, quite different from the real substrate in the ribosome.

The present paper is focused on the mechanism of the aminolysis of an ester in solution mimicking the peptide bond formation step that takes place in the ribosome. Thus, a realistic molecular model similar to the natural substrate used by ribosome, as shown in Scheme 2, has been used. The model, as already used in a previous study carried out in gas phase calculations and in solution by continuum models by one of us, and in our previous study focused on the analysis of the different conformations of zwitterion species in aqueous solution,[38] includes all the atoms involved in the different

Scheme 2. Molecular Model for the Nucleophilic Attack of the Amino Group on the Carbonyl Group of the Ester[a]
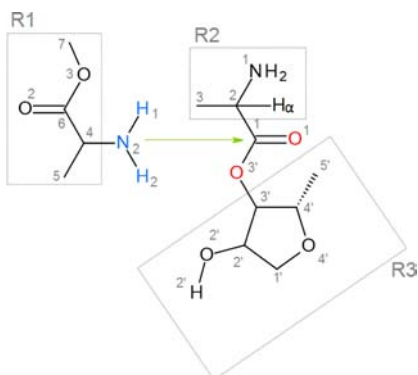
[a]R1, R2, and R3, as referred in Scheme 1.

proposed mechanisms, as well as the inherent constrain of the ribose ring that can govern the role of the hydroxyl group bound to C2′. The simplifications that have been considered are as follows: the atom C5′, which in the real system is bonded to the O atom of a phosphate in the RNA main chain, is represented by a methyl group. The base bonded to the C1′ is modeled by a H atom. The methyl groups C3 and C5 act as a model of the lateral chain of an amino acid. In the amino group N2, one of the H atoms takes the place of a polypeptide chain. Finally, the C7 methyl group models the ribose of tRNA.

This molecular model, treated by quantum mechanical methods, was solvated by a box of water molecules treated by a classical force field. Several mechanisms have been explored and compared. The concerted mechanism, mechanism 1 in Scheme 1, has been explored through different TSs: a direct 4-membered ring TS, a self-catalyzed mechanism by the hydroxyl group of the C2′ of the ribose through a 6-membered ring TS, and a mechanism involving an 8-membered ring TS by participation of both the C2′ hydroxyl group and a water molecule, have been also studied. To study this mechanism, one water molecule was also treated quantum mechanically. The stepwise mechanism through the neutral intermediate, mechanism 2 in Scheme 1, has been explored with participation of the C2′ hydroxyl group in the first step. Finally, mechanism 3 in Scheme 1, that takes part through a tetrahedral zwitterion intermediate, will be investigated. In this regard, we have recently published a study showing how, by means of the same methodology employed in the present paper, different conformations of the zwitterionic interacting complex could be opening the door for all the different proposed mechanisms.[38]

■ COMPUTATIONAL METHODS

The substrate and, when needed, a solvent water molecule, have been treated by the semiempirical AM1[39] Hamiltonian and by means of the M06-2X functional developed by Truhlar's group[40,41] with the standard 6-31+g(d,p) basis set, that includes diffuse functions. The full molecule described quantum mechanically was embedded in a box of water molecules ($100 \times 80 \times 80$ Å^3, 21 468 solvent water molecules

in total) treated by the TIP3P[42] force field, as implemented in fDYNAMO library.[43] Periodic boundary conditions were applied and a switched cutoff from 14.5 to 16 Å was employed for all nonbonded MM interactions. Water molecules were equilibrated by means of hybrid AM1/MM MD in the interaction reactant complex. Afterward, the mechanisms were explored by obtaining the corresponding potential energy surfaces (PESs) at the AM1/MM level. The transition state structures, at AM1/MM and M06-2X/MM levels of theory, were located by means of a micro-macro iteration scheme[44,45] from initial guess structure of the PES. The strategy is based on a partition of the full coordinates space of the system into a control space (the solute atoms) and complementary space subsets (the solvent atoms). Then, optimization of structures was efficiently carried out in coupled iterations over these two subspaces: at each step of the control space Hessian guided optimization, the rest of the system is kept fully relaxed merely using gradient vectors. Once the stationary points were located, they were characterized by frequency calculations to verify that the structures represent true minima or first-order saddle point on the AM1/MM and M06-2X/MM PESs. IRC paths were traced from the located TS at both levels of theory. One-dimensional (1D) and two-dimensional (2D) potentials of mean force (PMFs) were obtained using Umbrella Sampling (US).[46,47] Due to the high cost of these calculations, they were computed just at the AM1/MM level. Umbrella force constant of 2500 kcal·mol^{-1}·Å^{-2} was applied to the distinguished reaction coordinates (the antisymmetric combinations (C1−N2)−(C1−O3′) and (N2−H1)−(H1−O3′) for the 1D and 2D PMFs) to allow a perfect overlapping among the simulation windows. The weighted histogram analysis method (WHAM), combined with the umbrella sampling approach, was employed to scan the reaction coordinates. Ten picoseconds of relaxation and 20 ps of production, with a time step of 0.5 fs, using the velocity Verlet algorithm[48] to update the velocities, were run in each window. The PMFs were performed at 300 K, using the NVT ensemble.

In order to get the free energy profile at the M06-2X/MM level, free energy perturbation (FEP) methods were applied and the results compared with those obtained by means of the PMF. The configurations for which the free energy difference is estimated along the FEP correspond to structures obtained along the M06-2X/MM IRC and are thus characterized by a single coordinate, s:

$$s = \left[\sum_{i \in \text{QM}} m_i((x_i - x_{0i})^2 + (y_i - y_{0i})^2 + (z_i - z_{0i})^2) \right]^{1/2} \quad (1)$$

where x_{0i}, y_{0i}, z_{0i} are the Cartesian coordinates of the QM atoms in the transition state structure, whereas x_i, y_i, and z_i are the coordinates of a structure belonging to the IRC traced from this transition state structure, and m_i are the masses of the atoms. Within this treatment the free energy relative to the reactant can be expressed as a function of the s coordinate as:

$$\Delta G_{\text{FEP}}(s^R \to s^j)$$
$$= \Delta E_{\text{QM}}^{0,R \to j} + \Delta G_{\text{QM/MM}}^{R \to j}$$
$$= (E_{\text{QM}}^0(s^j) - E_{\text{QM}}^0(s^R)) - k_B T$$
$$\sum_{i=R}^{i=j-1} \ln \langle \exp \beta(E_{\text{QM/MM}}(s^{i+1}) - E_{\text{QM/MM}}(s^i)) \rangle_{\text{MM},i} \quad (2)$$

where E_{QM}^0 is the gas-phase energy of the QM subsystem computed at M06-2X level, k_B is the Boltzmann constant, T is the temperature, and $\beta = 1/k_B T$. The QM/MM interaction contribution to the free energy difference between two different values of s is obtained by averaging the QM/MM interaction energy (including the polarization energy) over all the MM coordinates of the system obtained for a particular value of the s coordinate. Ten picoseconds of relaxation and 20 ps of production, with a time step of 0.5 fs, were run in each window. The FEPs were performed at 300 K, using the NVT ensemble. For the remaining mechanisms, once the corresponding TSs were located and characterized at AM1/MM level, they were refined with the M06-2X/

MM potentials and the IRCs were traced and the FEPs computed as explained above.

Free energy contributions due to QM degrees of freedom were introduced treating them as harmonic vibrations, using the following expression:

$$G_{\text{QM,vib}} = \sum_{i=1}^{m} \frac{1}{2} h\nu_i + \sum_{i=1}^{m} RT \ln(1 - e^{-h\nu_i/k_B T})$$
$$= \text{ZPE} + G'_{\text{QM,vib}}(T) \quad (3)$$

where m is the number of vibrational modes to be considered and ν_i the fundamental frequency associated with each one of these modes. The first term is the well-known zero-point energy, while the second one contains the thermal contribution of the vibrations to the molecular free energy. The correction to the activation free energy is obtained as the difference between the free energy of the transition state and the reactant states:

$$\Delta\Delta G_{\text{vib}} = \Delta G_{\text{vib}}^{\text{TS}} - \Delta G_{\text{vib}}^{\text{R}} = \Delta\text{ZPE} + \Delta G'_{\text{QM,vib}}(T) \quad (4)$$

Since the six lowest frequency modes of the transition state and the reactant structures correspond to very low frequency librational motions,[49] their contribution to the vibrational correction (eq 4) is expected to be small, and consequently, we omit these modes. Then, the correction is calculated over the $3N - 6$ (in the reactant state) or $3N - 7$ (in the transition state) frequency modes, with N being the number of atoms in the QM subsystems.

Finally, from the stationary structures of the rate limiting transition states and the solvated separated species in reactants state at the highest level of theory, M06-2X/MM, the rigid-rotor/harmonic-oscillator approximation was used with the fDYNAMO library to calculate semiclassical kinetic isotope effects, KIEs, without scaling of vibrational frequencies, as explained and applied in previous papers.[50,51] The subset of atoms used to define the Hessian for these KIE calculations were those of the QM region plus the water molecules of the first solvation shell interacting with the carbonyl oxygen O1 atom, consistent with the "cut-off rule" and the local nature of isotope effects.[52]

■ RESULTS AND DISCUSSION

The first explored reaction correspond to the concerted mechanism that takes place through a 4-member ring TS, mechanism 1 in Scheme 1. The PMF for this concerted mechanism has been obtained by using the antisymmetric combination of breaking and forming bonds, C1−O3′ and C1−N2, as the distinguished reaction coordinate. The resulting free energy profile is presented in Figure 1a. As observed in the profile, a very shallow intermediate, ZW, is obtained prior reaching the rate limiting TS, TS-4. In this last structure, the C1−O3′ breaking bond and the C1−N2 forming bond processes are in a very advanced stage as reflected by the value of their respective distances (Figure 1b). On the contrary, the proton of the amine group, H1, is still bonded to the nitrogen atom although already oriented for the transfer to the O3′ atom. Interestingly, the C1−O1 bond at TS-4 presents the standard distance of a carbonyl double bond, after having been elongated at the ZW intermediate (see Figure 1c). The elongation of the C1−O1 distance in ZW is associated with a negative charge transfer from the nucleophile to the O1 atom.[38] This, together with a preliminary stage of the C1−N2 forming bond, is characteristic of an addition tetrahedral zwitterionic species. The stability of this zwitterion is very modest according to the backward free energy barrier to reactants (less than 1 kcal·mol^{-1}), but it is assisted by hydrogen bond interactions established between the negatively charged O1 and water molecules of the solvent.
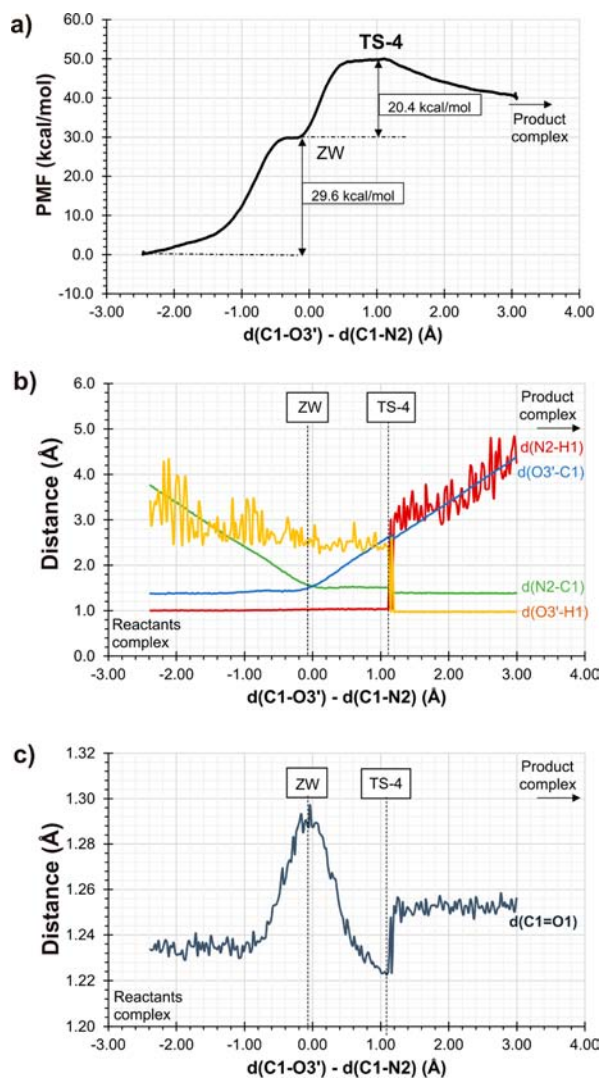
Figure 1. (a) 1D PMF for the noncatalyzed concerted mechanism obtained at AM1/MM level, (b) evolution of averaged interatomic distances along the PMF, and (c) amplified plot of evolution of averaged C1−O1 interatomic distance along the PMF.
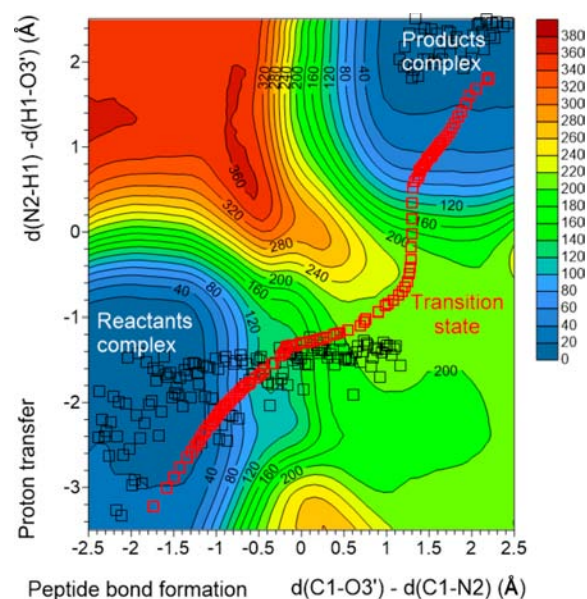

Figure 2. 2D PMF for the mechanism 1 obtained at AM1/MM level. Averaged values of the two antisymmetric coordinates obtained along the 1D PMF (black squares) and the FEP method (red squares). Values of isoenergetic curves are in $kJ \cdot mol^{-1}$.

Considering the amount of variables that are involved in the process, the fact that some of them (those associated to the proton transfer) are not explicitly controlled with the distinguished reaction coordinate used in the 1D PMF, and the large asynchronicity on the evolution of the distances (very advanced N2−C1 bond forming and C1−O3′ breaking bond and very retarded proton transfer), a 2D PMF has been computed. The two coordinates used to generate the free energy profile were the two antisymmetric distances: $d(C1−O3′)−d(C1−N2)$ and $d(N2−H1)−d(H1−O3′)$. The result is presented in Figure 2.

In Figure 2, the lower left corner corresponds to reactants while the upper right corner corresponds to products. The quadratic region of the TS corresponds to structures where the C1−N2 forming bond and C1−O3′ breaking bond are in a very advanced stage of the process, while the proton of the amine group is still bonded to the nitrogen atom. This is in agreement with the features of the TS-4 located in the 1D-PMF. Inspection of the evolution of the averaged values of the two antisymmetric coordinates obtained in the 1D PMF on the 2D PMF (black squares in Figure 2) shows that the $d(C1−$

$O3′)−d(C1−N2)$ coordinate used in the 1D PMF presented in Figure 1 correctly represents the evolution of the system from the reactants complex to TS-4. However, this coordinate is no longer useful to represent the change from TS-4 to products because this process is dominated by the proton transfer and, since the coordinates defining its position were not controlled in the 1D PMF a significant discontinuity from the TS region to the product basin is obtained. This effect was already observed in Figure 1b, where an important jump on N2−H1 and O3′−H1 distances take place once the TS-4 is crossed. Another effect derived from the lack of control on the internal coordinates related with the proton transfer is the large dispersion observed for the proton transfer coordinate in the averaged structures obtained from the simulation windows of the 1D PMF. Again, fluctuation of O3′−H1 and N2−H1 distances at negative and positive values of the x-axis of Figure 1b was indicative of this dispersion. As observed, there is a clear hysteresis effect when the reaction coordinate is controlled by a limited number of internal coordinates which could lead to a slight overestimation of the free energy barrier. Keeping in mind that higher-level calculations are desirable to explore this and the rest of proposed mechanisms, the less computationally demanding FEP method has been applied at AM1/MM level using the QM coordinates generated along the IRC path traced down from a representative TS-4 structure. The resulting AM1/MM FEP is presented in Figure 3a. As can be observed, the topology is very close to the one obtained in the 1D PMF presented in Figure 1a, with the exception that the swallow minima corresponding to the zwitterionic species located in the 1D PMF is now a shoulder. The relative free energy values of this shoulder and the rate limiting TS-4 are, nevertheless, very similar to the values derived from the 1D PMF. The evolution of the key interatomic distances (Figure 3c and e) is also in very good agreement with the results obtained from the 1D PMF (Figure 1b and c). The evolution of the antisymmetric combination of C1−O3′ and C1−N2 interatomic distances along the AM1/MM FEP is projected on the 2D PMF plotted
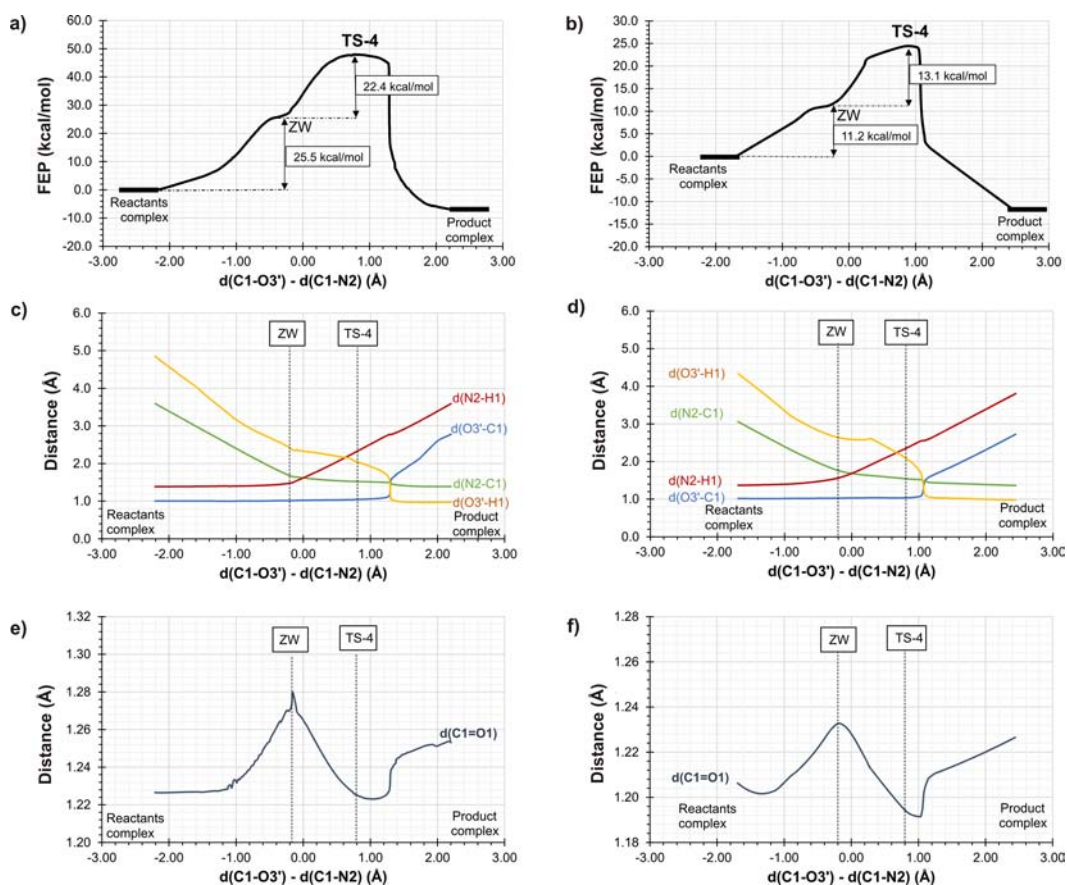
Figure 3. Free energy profiles obtained by means of FEP method for the concerted mechanism 1 obtained at (a) AM1/MM and (b) M06-2X/MM levels of theory. Panels (c) and (e) correspond to the evolution of averaged interatomic distances and amplified plot of evolution of averaged C1–O1 interatomic distance, respectively, obtained from the AM1/MM FEP calculations, while panels (d) and (f) show the corresponding values at M06-2X/MM level.

in Figure 2 as red squares. Once again, the reaction proceeds from the lower left corner to the upper right corner of the surface. Obviously, since the solute coordinates of the FEP profile correspond to the ones generated along the QM/MM IRC path, the projection of evolution of the values derived from the FEP on the 2D PMF is smoother than the one observed from the values generated along the 1D PMF. In particular, the proton transfer coordinate is well controlled avoiding then any hysteresis problem associated to the use of a simple geometrical coordinate as distinguished coordinate. These results confirm the nature of TS-4 as the TS for the concerted process, the existence of zwitterionic species located along the reaction path, and the capabilities of the less computationally demanding FEP technique.

Keeping in mind this observed agreement between the profiles obtained by means of FEP and PMF techniques, the FEP method has been chosen to get the free energy profiles within higher level quantum Hamiltonians. As explained in the Computational Methods section, the hybrid functional M06-2X has been chosen to describe the QM atoms. Thus, once located and optimized a TS structure at the M06-2X/MM level, and traced the IRC down to reactants and products valleys, the generated geometries along the IRC at this level of theory were used to compute the FEP. The shape of the free energy profile generated by the M06-2X/MM FEP method (Figure 3b) appears to be similar to the one obtained with the AM1/MM method (Figure 3a), and to the 1D PMF obtained at AM1/

MM level (Figure 1a), but with quite different values of the free energy changes.

The free energy barrier obtained at M06-2X/MM (24.3 kcal·mol^{-1}), significantly lower than the one deduced from the AM1/MM calculations (50.0 and 47.9 kcal·mol^{-1} from the 1D-PMF and FEP calculations, respectively), is very close to the experimentally measured free energy barrier of 23.5 ± 0.7 kcal·mol^{-1} of the uncatalyzed reaction of N-formylphenylalanine trifluoroethyl ester with glycinamide (the amine presenting the closest pK_a value to the model used in the present study) measured at 25 °C.[53] Nevertheless, this almost quantitative agreement between experiments and computational predictions has to be considered with caution, since the IRCs, both at the AM1/MM and M06-2X/MM level, did not finish in the completely solvent-separated species but in an interaction reactant complex. Estimation of the free energy difference between the reactant complex and the fully solvated separated species, computed within a polarizable continuum model for the same reaction complex as the one used in the present study and with the same functional, M06-2X, rendered values in the range 4–7 kcal·mol^{-1}.[28] This free energy difference refers to a process of association of two fragments and thus depends on the choice of the standard state, which in this case it is 1 M. Thus, our present prediction would be slightly overestimated, by comparison with the experimental data. The TS structures optimized at the M06-2X/MM level are presented in Figure 4. It is important to point out that neither the free M06-2X/MM energy profile nor the IRC traced down
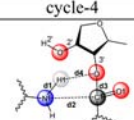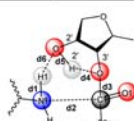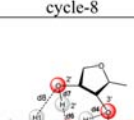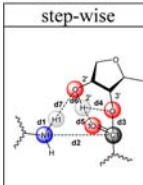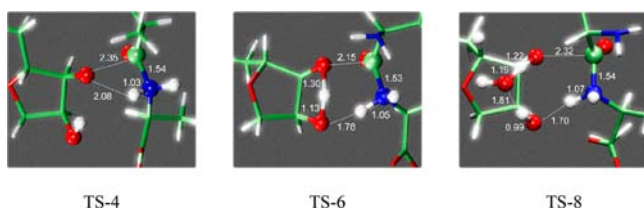
Figure 4. TSs located at M06-2X/MM level for the concerted mechanism 1. TS-4, 4-membered ring TS; TS-6, 6-membered ring TS with participation of the hydroxyl group of the C2′ of the ribose; and TS-8, 8-membered ring TS with participation of a water molecule and the C2′ hydroxyl group. Key distances are in Å.

Table 1. Key Distances (in Å) Obtained for the Zwitterion, Intermediate, and TS Species at M06-2X/TIP3P

cycle-4			ZW	TS
		d1	1.03	1.03
		d2	1.72	1.54
		d3	1.60	2.35
		d4	2.61	2.08
		d(C1-O1)	1.23	1.19
cycle-6				
		d1	1.03	1.05
		d2	1.67	1.53
		d3	1.51	2.15
		d4	1.72	1.30
		d5	0.99	1.13
		d6	1.99	1.78
		d(C1-O1)	1.27	1.22
cycle-8				
		d1	1.03	1.07
		d2	1.79	1.54
		d3	1.53	2.32
		d4	1.63	1.22
		d5	0.99	1.19
		d6	2.11	1.81
		d7	0.97	0.99
		d8	1.81	1.70
		d(C1-O1)	1.23	1.19

step-wise		ZW	TS1	II	TS2
	d1	1.03	1.20	3.03	4.35
	d2	1.71	1.53	1.43	1.31
	d3	1.42	1.39	1.42	2.12
	d4	2.60	2.56	2.62	1.82
	d5	1.99	1.04	0.98	0.99
	d6	0.97	1.49	1.93	2.12
	d7	3.30	1.33	0.97	0.97
	d(C1-O1)	1.29	1.39	1.42	1.34

from the TS-4 show any local minimum between the reactants complex and TS. Nevertheless, a clear shoulder is shown in both cases in a region located at a value of the antisymmetric combination of the C1−O3′/C1−N2 bond distance equal to −0.75 Å. Electronic and geometrical analysis of this structures confirms its zwitterionic character. Population analysis of the zwitterionic structure reveals that O1 is highly negatively charged (−1.11 au), which is stabilized by an intramolecular hydrogen bond established with the C2′ hydroxyl group and two intermolecular hydrogen bonds with two water molecules. The length of the C1 carbonyl double bond is significantly elongated, 1.23 Å, by comparison with the value observed in the reactant complex (1.20 Å) and in the TS-4 (1.19 Å). The positive charge developed in the NH$_2$-group is stabilized by an intermolecular hydrogen bond established with a water molecule and an intramolecular hydrogen bond with the carbonyl group of the fragment of the molecular model mimicking the amino acid. This zwitterionic intermediate is describing a preliminary stage of the N2−C1 bond forming, the C1−O3′ breaking bond is in a very early stage of the process, and one of the protons of the amino group is already oriented for being transferred to the ester oxygen O3′ atom. In contrast, population analysis of the O1 atom in the TS-4 structure displays a relatively low charge (−0.52 au) and, as commented, the C1−O1 distance corresponds to a standard carbonyl double bond. The C1−O3′ breaking bond is very advanced in TS-4 (2.35 Å) and, considering the associated charge transfer from this O1 atom (charge on O3′ and C1 atoms in the TS-4 are −0.99 and 0.82 au, respectively), reveals a heterolytic bond cleavage. Altogether, it seems that TS-4 is reasonably well described as an ionic pair with a charge on the ribose ring equal to −0.93 au and a positive charge on the remaining fragment of +0.93 au.

Once the concerted mechanism has been explored through a 4-membered ring TS, TS-4, and it is shown how the FEP method can render reasonable and nearly identical free energy profiles than 2D PMF, the other two proposed concerted mechanisms will be studied using this methodology. They are the self-catalyzed mechanism by the hydroxyl group of the C2′ of the ribose, that takes place through a 6-membered ring TS, and a mechanism involving an 8-membered ring TS, by participation of both a water molecule and the C2′ hydroxyl group. The localized TSs are depicted in Figure 4, and a list of key distances are reported in Table 1. According to these results, it can be observed how the distances between C1−N2 atoms are nearly identical in the three TSs. Similar behavior is observed in the N2−H1 distances. On the contrary, the C1−O3′ breaking bond appears in a much less advanced stage of the reaction in the 6-membered TS (2.15 Å) than in the 4 and 8-membered ring TSs (2.35 and 2.32 Å, respectively). By

comparison between TS-6 and TS-8, this result is obviously related with the distance between the O3′ atom and the accepting proton from the vicinal hydroxyl group and from the water molecule, respectively. The more transferred is the proton to O3′ atom, the more advanced the breaking C1−O3′ bond. In the case of TS-4, this trend is not observed since the proton is transferred from N1 and then it is also related with the C1−N2 distance. Moreover, by comparison of all these distances with the ones obtained in previous gas phase results,[28] it can be observed how the TSs located in the present study describe a less advanced proton transfer to O3′ in all the cases. This is due to the fact that, as mentioned, the water solvent molecules stabilize separated charges and, consequently, delay the charge transfer, that is, the proton transfer. Population analysis of the three TSs confirms this prediction. In fact, apart from TS-4, TS-8 is also reasonably well described as an ionic pair with a charge on the ribose ring equal to −0.90 au and a positive charge on the remaining fragment of +0.90 au. Both TSs present a significant degree of C1−O3′ breaking bond. Slightly smaller values are observed in TS-6 (−0.80 and +0.80 au), which is correlated with a shorter C1−O3′ bond than TS-4 and TS-8.

Interestingly, Wallin and Åqvist also located a 6- and an 8-membered TSs at DFT level with the B3LYP functional using a cluster model of about 80 atoms that mimic the active site of ribosome.[6] Nevertheless, some important differences can be detected. For instance, the C1−O3′ and C1−N2 distances in our TS-6 appear to be in a slightly more advance stage of the reaction, while both proton transfers are less advanced: H1 from N1 to O2′ and H2′ from O2′ to O3′. These differences can be attributed to the different environment of both studies, since the aqueous reaction field favors charged separated species then retarding the proton transfers. A more complex trend is observed if comparing our TS-8 structure with the
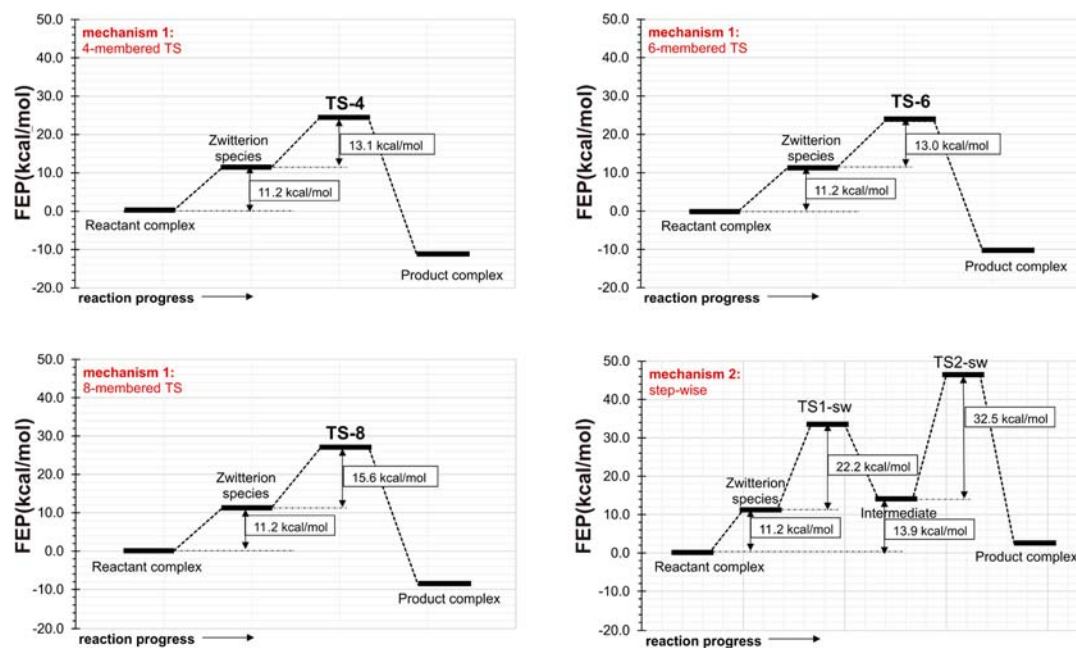
Figure 5. M06-2X/MM free energy profiles obtained by means of FEP methods for the different mechanisms of the nonenzymatic peptide bond formation; mechanism 1 (panels a−c) and stepwise mechanism (panel d).

three models Wallin and Åqvist used to locate the 8-membered TSs (with a single screening oxyanion water, with a doubly screened oxyanion or naked). In any case, the nucleophilic attack of N2 to C1 is less advanced on our TS-8 than in all their TSs, which is reasonably associated with a less advanced stage of the H1 transfer from the N2 to O2′. According to their calculations, the breaking ester bond (C1−O3′) and the relative position of the other two protons involved in the 8-membered TS appeared to be strongly dependent on the model. Regarding H1 and H2′ proton transfers, they are less advanced in our study than in their three models, again in agreement with the expected role of aqueous reaction field favoring charged separated species. Then, it is not surprising that these differences between our TS-6 and TS-8 structures located in aqueous solution and the structures located by Wallin and Åqvist in a ribosome-like environment result in a different relative energy ordering of the TSs.

The FEP method has then be used at the M06-2X/MM level from the structures generated on the IRC traced down to reactants and products from the localized QM/MM TSs. The resulting free energy profiles are plotted in Figure 5. Interestingly, analysis of the evolution of key interatomic distances along the IRCs from TS to reactant complex, in particular C1−N2, C1−O1 and C1−O3′ distances, allows concluding the presence of zwitterion character species from reactants to TS in all mechanisms (see Table 1). This structure appears as a shoulder on the free energy profile corresponding to the mechanism that take place through TS-4 and TS-8 but as a metastable intermediate in the mechanism through TS-6. In this case, an almost barrier-less process takes place from this minimum to reactants on the free energy surface. The zwitterion character of these structures, displayed in Figure 6, has been confirmed by the analysis of interatomic distances and charges. In all cases, the accumulated charged in O1 is stabilized by at least two hydrogen bond interactions with water molecules of the solvent, as observed in our previous study.[38] In that work, where we explored different conformations of
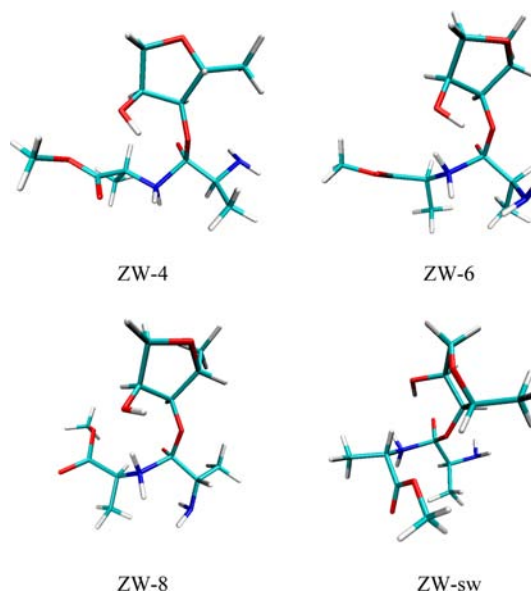

Figure 6. Zwitterion species, ZWs, located at M06-2X/MM level on the reaction path of the concerted mechanisms (ZW-4, ZW-6, and ZW-8) and the stepwise mechanism (ZW-sw). Water solvent molecules are not displayed for clarity purposes.

zwitterion species during QM/MM MD simulations constraining the antisymmetric combination of C1−O3′ and C1−N2 distance, significantly different conformers were detected along the MD simulation. According to this result, it was proposed that the different zwitterion conformers could open the door to different mechanistic paths for the ester aminolysis. In the present study, where the full reaction profiles have been explored and the evolution of key geometrical parameters analyzed from the TSs to reactants, the appearance of different conformers with zwitterionic character has been confirmed. Representative structures of these families of conformers, selected and optimized at M06-2X/MM level in our previous

study,[38] are equivalent to the zwitterionic structures obtained in the concerted mechanisms taking place through TS-4, TS-6, and TS-8 (see Figure 6). Consequently, the difference in the energy barrier between these paths will be determined by the energy difference between these zwitterion structures and their corresponding TSs. According to the computed FEPs, these are, 13.1, 13.0, and 15.6 kcal·mol^{-1} for the 4-, 6-, and 8-membered ring TSs, respectively.

The free energy difference between the zwitterion species and the reactant complex is 11.2 kcal·mol^{-1}. Adding this contribution to the free energy difference between zwitterions and their respective TSs, we estimated that the total free energy barriers from the reactant complex to be 24.3, 24.2, and 26.8 kcal·mol^{-1} for the 4-, 6-, and 8-membered ring TSs, respectively. The vibrational corrections computed according to eq 4 amount to 1.1, 1.2, and 2.5 kcal·mol^{-1} for the 4-, 6-, and 8-membered ring TSs, respectively. These values are basically derived from the zero point vibrational terms. Then our best estimations for the activation free energies for each of the explored mechanism as measured from the reactant complex are 23.2, 23.0, and 24.3 kcal·mol^{-1} for the 4-, 6-, and 8-membered ring TSs, respectively. All in all, negligible differences have been obtained between the energy barriers of the first two concerted mechanisms (23.2 and 23.0 kcal·mol^{-1}). The reaction through the 8-membered ring TS would be only slightly less favorable (free energy barrier of 24.3 kcal·mol^{-1}).

The stepwise mechanism, mechanism 2 in Scheme 1, involves participation of the proton transfer from the amino group, N2, to the carbonyl O1 atom, concomitant with the C1—N2 forming bond. In the second step, the proton is transferred to the O3′ while the C1—O3′ bond breaks. The two TSs are depicted in Figure 7. As observed in TS1-sw, the
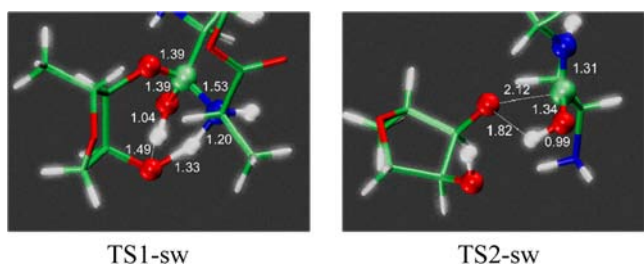

Figure 7. TSs located at M06-2X/MM level for the stepwise mechanism. Key distances are in Å.

proton transfer does not take place through a direct 4-membered ring, but with participation of the vicinal C2′ hydroxyl group (see Table 1 for detailed information of the key interatomic distances). The second step is controlled by TS2-sw, depicted in Figure 7, that corresponds to the C1—O3 breaking bond process concertedly with the proton transfer. According to our M06-2X/MM free energy calculations (see Figure 5), the second step would be the rate limiting step.

Interestingly, the IRC traced down from the TS1-sw to reactants renders an intermediate that, by inspection of distances and charges, revealed to be an addition tetrahedral zwitterion intermediate. The structure, depicted in Figure 6 as ZW-sw, is equivalent to one of the conformations of zwitterion species described in our previous study that were generated from constrained long QM/MM MD simulations.[38] From the energetic point of view, and according to the free energy profile depicted in Figure 5, the stepwise mechanism could be clearly

discarded since the rate limiting step presents a barrier (46.4 kcal·mol^{-1}) much higher than the ones obtained in the concerted mechanisms.

Kinetic Isotope Effects. In order to confirm our predictions, KIEs have been computed from the TS structures located on the four different pathways and compared with experimental data reported by Strobel and co-workers for aminolysis by hydroxylamine at pH 8.0.[18] The results are listed in Table 2.

Table 2. M06-2X/TIP3P KIEs Calculated at 300 K

	cycle-4	cycle-6	cycle-8	step-wise	exp
1-[^{13}C]	1.036	1.039	1.024	1.045	1.027 ± 0.005[a]
1-[^{18}O]	1.007	0.995	1.008	1.017	1.037 ± 0.007[a]
3′-[^{18}O]	1.066	1.050	1.031	1.059	1.029 ± 0.006[a]
2′-[^{18}O]	1.000	0.981	0.992	0.974	1.007 ± 0.003[a]
2′-[^{2}H]	1.059	2.973	0.991	1.455	
α-H-[^{2}H]	1.091	0.962	0.941	1.019	0.962 ± 0.008[a]
1-[^{15}N]	0.970	0.962	0.971	0.964	0.990 ± 0.001[b]

[a]Data from ref 18. [b]Data from ref 15.

By comparison with the experimental data, there is a qualitative agreement between experiments and computations for the effects of carbonyl carbon and ester oxygen isotopes substitutions (1-[^{13}C] and 3′-[^{18}O], respectively) for whatever considered mechanism. According to the rate limiting TSs, the large normal isotope 3′-[^{18}O] and 1-[^{13}C] effects are in agreement with the ester C—O breaking bond for the first three mechanisms and the breakdown of the tetrahedral intermediate in the stepwise mechanism. Lower values are observed for the 1-[^{13}C] due to the fact that the C—N bond is almost completely formed in TS-4, TS-6, and TS-8: C1—N2 distance in the TSs of the first three mechanisms is between 1.53 and 1.54 Å, while in products it is 1.3–1.4 Å. Since C1—N2 distance at TS2-sw is already at values corresponding to products, 1.31 Å, the 4.5% normal effect on C1 computed for this mechanism must be explained considering this atom is involved in the ester breaking bond but also in the transfer of proton from O1 to O3′. Thus, while C1—O3′ distance on TS2-sw is similar to the values on TS-4, TS-6, and TS-8, the C1—O1 distance is significantly larger (see Table 1). It is important to point out that Strobel and co-workers used two isomers of CCApcb and only in one of them the 3′-oxygen was the leaving group. Since their observations come from both isomers, it explains our higher predicted values. Thus, and considering the experimental errors and the theoretical deviations, these two isotope substitutions could not be used to discard any of the studied mechanisms, unless a more detailed analysis at quantitative level was done. In such cases, the values obtained in the case of the mechanism through the TS-8 can be considered to be at almost quantitatively agreement with experimental data.

The inverse 3.8% α-deuterium isotope effect (αH-[^{2}H]) measured by Strobel and co-workers was attributed to a substantial sp^3 character on the aminolysis TS.[18] As observed in Table 2, only TS-6 and TS-8 would render the same trend, while TS-4 and stepwise TS-sw give normal KIEs. Thus, the origin of inverse effect can not be attributed to the sp^3 character of α-C, since all four TS present the same hybridization states, as revealed by calculations based on the local geometry of these carbon atoms and their directly bonded neighboring atoms (ca. sp$^{3.0}$ for the four TSs).[54] Instead, differences in the interactions of this proton atom with O1 and O3′ in the TSs could explain

the different observed trends. Thus, as observed in Figure 4, α-H is oriented to O1 in TS-6 and to O3′ in TS-8, while in TS-4 the $C\alpha$-H bond is pointing out to the solvent. Keeping in mind the charge developed in these two oxygen atoms in the TSs, and despite $C\alpha$-H bond is not a polar bond, the inverse effect can be explained due to the additional constrains imposed by these interactions. The distance between α-H and O1 was 2.59 Å in TS-6, while the distance between α-H and O3′ was 2.38 Å in TS-8.

Small normal effect of 0.7% was experimentally measured for the 2′-[^{18}O] substitution. Participation of the vicinal hydroxyl group is responsible of the predicted inverse effect observed in TS-6 and TS-8. A first analysis based on schematic representations of TSs would suggest that TS-4 and TS2-sw should render no effects after 2′-[^{18}O] substitution, but, as observed in Figures 4 and 7, this hydroxyl group is not entirely alien to the changes that take place in the TS. Additional weak interactions are established between this group and the O3′ atom in TS-4 and TS-sw, thus explaining the absence of KIE in the former or a small inverse effect in the later. Also, it must be kept in mind that the reaction is studied in solution and, since a charge transfer is involved during the reaction, changes in interactions with water molecules of the solvent have to be considered to explain the observed effects. Large effects of surrounding water on phosphate deprotonation reactions in solution was already observed by Åqvist and co-workers and attributed to the strong solute−solvent interactions.[55] In fact, if KIEs calculations are done without including those water molecules hydrogen bonded to O1 into the evaluation of the Hessian, this is without considering the changes in frequencies of water−solute intermolecular interactions, a normal effect of 0.4% is obtained in TS-4. Anyway, conclusions must be taken with caution keeping in mind the small effects computed in all four mechanisms and in experimentally measurements and that, as mentioned by Strobel and co-workers, the observed rates for aminolysis of the two isomers by may not be equal.

All predicted values of the carbonyl ^{18}O isotope effect appear to be far from the high 3.7% value determined experimentally by Strobel and co-workers. Prediction for the carbonyl 1-[^{18}O] effect computed from the TS-4, TS-8 and stepwise mechanisms agree with the normal effect experimentally observed, while mechanism through TS-6 render an inverse KIE. In order to analyze this effect, not only intramolecular distances, but also the charge evolved on O1 atom, and consequently interatomic distances with solvent water molecules, have to be considered. Thus, while the C1−O1 distances are lengthened at the concerted TSs compared to reactants, there is a shortening of hydrogen bond distances between O1 and water molecules that is associated with the charge migration associated to the reaction. The result is that instead of inverse KIEs that would be expected if only C1−O1 distance were taken into account for the analysis, normal effects are computed for TS-4 and TS-8. In fact, calculations of KIEs carried out without considering changes of frequencies derived from first shell of water molecules, as performed above to analyze the 2′-[^{18}O] KIEs, render also inverse KIEs for TS-4 and TS-8. The stepwise mechanism provides, however, a normal effect of 1.7% that could be considered in better agreement with the 3.7% obtained experimentally. In this case, the C1−O1 distance in TS2-sw (1.34 Å) is dramatically longer than in the concerted TSs (1.19−1.22 Å) and becomes the most important contribution to the normal effect. Strobel and co-workers performed gas phase calculations to fit the experimental normal

kinetic effects. In their models, due to the fact that they did not considered solvent effects, the C1−O1 distance had to be elongated up to 1.37 Å, far from the values obtained in our QM/MM calculations and close to a standard C−O distance of a hydroxyl group. In all the predicted QM/MM calculations, KIEs are much closer to unity due to the compensation by solvent−solute interactions, but it is also probably that the lack of agreement between experiments and theory comes from the fact that different reactions are under study: the aminolysis was experimentally studied with a hydroxylamine, different to the nucleophile used in our study that mimics an aminoacid. At this point, Strobel and co-workers mentioned that, because hydroxyl-amine is a better leaving group than the 3′-oxygen, formation of the zwitterion tetrahedral species could resolve back into reactants instead of products.[56] Then, the observed isotope effect could be equal to the product of the equilibrium effect on formation of the ZW and the kinetic isotope effect on its breakdown. This behavior has been observed for other aminolysis reactions with good nucleophiles.[57,58] In such a case, effects coming from formation of the zwitterionic species would contribute to the overall KIE for carbonyl [^{18}O] substitution and, keeping in mind that C1−O1 distance reaches a maximum at this point, higher effects could be expected. All in all, comparison between experiments and our calculations have to be done with caution.

Finally, we have computed the effect of the incoming nucleophile nitrogen isotope substitution (1-[^{15}N]). This is a key probe for the proposed mechanisms according to the different values experimentally obtained in the catalyzed and uncatalysed reactions. Thus, Brønsted linear free energy relationships suggest that the nucleophile is neutral at the TS of the ribosome-catalyzed reaction, while it would be positively charged for the uncatalyzed aminolysis reaction.[59] In other words, the nitrogen deprotonation would occur simultaneously with the formation of the C−N bond in the ribosomal catalyzed reaction, while in solution the proton transfer would occurs after the nucleophilic attack. This hypothesis of different mechanisms in ribosome and in aqueous solution has been supported by measurements of 1-[^{15}N] KIEs rendering a normal effect in the ribosome[17,60] and inverse in different ester aminolysis reactions in solution (0.996 for the acylation of aniline[61] and 0.990 for the aminolysis of methyl formate by hydrazine at pH 8).[15]

The inverse 1-[^{15}N] KIE values obtained in our calculations for all the mechanisms would be in agreement with the experimental evidence confirming that the ribosome promotes peptide bond formation by a mechanism that could differ in its details from an uncatalyzed aminolysis reaction in solution.[17,18,60] In the paper of Wallin and Åqvist,[6] inverse KIEs were obtained for the 1-[^{15}N] for both two examined mechanisms; through a six-membered TS and an eight-membered TS, with a ribosome-like model. Keeping in mind that interpretation of KIEs in condensed media is not always intuitive, these results would be indicative of a model that could not catch all the essentials of the macromolecular machine responsible for protein synthesis in cells.

■ CONCLUSIONS

QM/MM MD simulations have been performed describing the QM region at semiempirical AM1 and by DFT within the M06-2X functional, in order to explore the aminolysis of an ester in aqueous solution. The system employed in the present study is similar to the natural substrate used by ribosome for the

Scheme 3. Proposed Reaction Mechanism for the Aminolysis of Esters in Aqueous Solution Obtained from our QM/MM MD Simulations
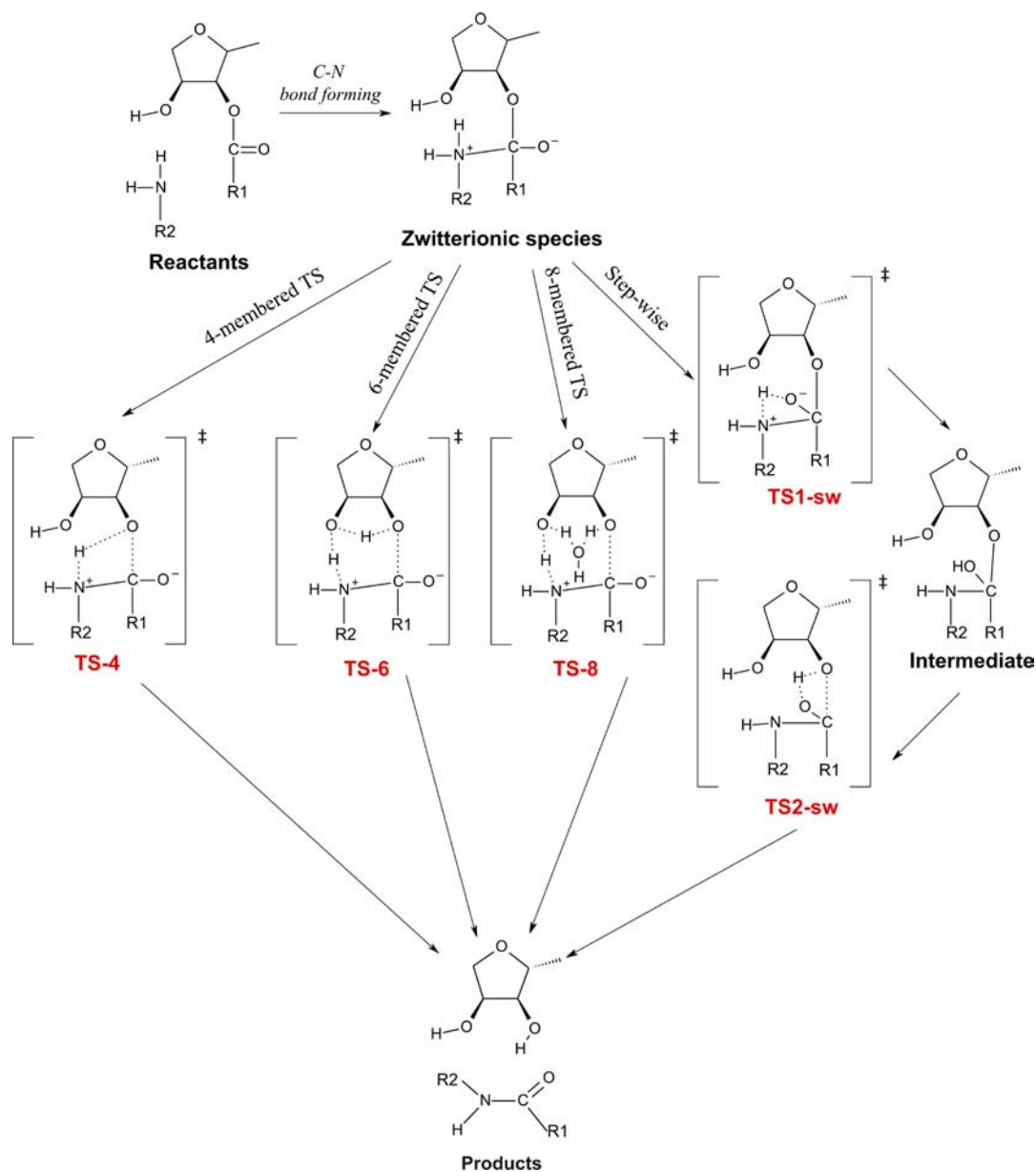
peptide bond formation step. The different mechanisms proposed in the literature have been explored, and the comparison of the resulting free energy profiles, obtained by means of US and FEP techniques, allows stating the molecular mechanism in aqueous solution. The first conclusion that can be derived from our calculations, with hybrid AM1/MM potentials, is that both US and FEP techniques converge to the same results within an almost quantitative agreement for a first tested mechanism. These positive conclusions are the bedrock to use the less computing demanding FEP methods to study the rest of the mechanisms, which allows improving the Hamiltonian of the QM region of the system. From the mechanistic point of view, the results can be summarized in Scheme 3. As observed, it appears that the formation of a transient zwitterion adduct is a preliminary step required for any of the mechanism previously proposed in the literature. This result confirms the prediction based on previous AM1/MM MD simulations carried out on zwitterionic species.[38] The

electrostatic effect of the solvent on the aminolysis of esters in solution, simulated by this discrete QM/MM model, favors the separation of charges of the system in the TS by delaying the proton transfer and advancing the heterolytic ester breaking bond.

After formation of these zwitterionic species, two different kinds of mechanisms were found: (1) concerted mechanism and (2) stepwise mechanism, that takes place through a neutral intermediate. In turn, the concerted mechanism can take place in a noncatalyzed way, through a 4-membered TS, or in a catalyzed way with participation of the hydroxyl group of the C2′ of the ribose through a 6-membered ring TS, or involving an 8-membered ring TS by participation of the C2′ hydroxyl group and a water molecule.

The comparative analysis of the free energy profiles indicates that the most favorable mechanisms would be the concerted ones taking place through a 4- or 6-membered ring TS (free energy barriers of 23.2 and 23.0 kcal·mol^{-1}, respectively). The

hydroxyl group of the C2′ of the ribose does not appear to have a significant catalytic effect, according to the negligible differences in the barriers. This conclusion agrees with previous quantum mechanical calculations,[28] and the overall free energy barrier with respect to the reactants complex is very close to experimental data: 23.5 ± 0.7 kcal·mol^{-1} for the uncatalyzed reaction of N-formylphenylalanine trifluoroethyl ester with glycinamide measured at 25 °C.[53] The barrier of the mechanism through an 8-membered ring TS, 24.3 kcal·mol^{-1}, is only 1.3 kcal·mol^{-1} higher than the lowest energy barrier. The rate limiting step of the stepwise mechanism indicates that this last pathway is clearly unfavorable, keeping in mind the obtained free energy barrier (46.4 kcal·mol^{-1}).

Thus, considering that similar free energy barriers were obtained for the three concerted mechanisms, KIEs were computed and compared with experimental data on a similar system. The results show that only the mechanism that takes place through an 8-membered ring TS, TS-8, can qualitatively reproduce the KIE of all experimentally tested substitutions but the small normal effect measured for the 2′-[^{18}O] substitution effect. In fact, none of the mechanisms provide the 0.7% experimentally measured normal effect for this isotopic substitution. Nevertheless, keeping in mind the small effect, measured or computed, the associated errors and standard deviations, and the fact that the experimental system and the computational model were different (in particular the nucleophile species), this discrepancy can be considered as acceptable. Deuterium substitution of the proton of the vicinal hydroxyl group could be a conclusive test to differentiate between these two considered as catalyzed mechanisms, since our calculations predict dramatic differences depending on the mechanism. Nevertheless, interchange of not only this proton but also protons of amine groups with deuterated solvent water molecules would probably make a very complex interpretation of the experimental results.

Finally, it is important to consider that the obtained trend in the barriers could change for the reaction in the ribosome keeping in mind the negative value of the entropy terms in solution that will not be observed in the ribosome due to ability of the rRNA to orient and position substrates. In fact, according to previous experimental studies of Rodnina and co-workers[62,63] and of Schroeder and Wolfenden,[53] the ribosome would be catalyzing the peptide bond formation in nature by means of an entropy trap. Moreover, as reported by Warshel and co-workers[34] and by Trobo and Åqvist,[4] apart from a solute configurational entropy, there would be a significant entropy contribution of the environment or solvation entropy; the nonfavorable solvent reorganization in the uncatalyzed water reaction would not take place in the preorganized protein environment when the system evolves from reactants to the TS. Then, a significant contribution of the reduction of the free energy barrier in the ribosome, compared with its counterpart reaction in solution, would be due to the reduction of the unfavorable entropic term, considered a sum of the solute and environment terms. Then, keeping in mind the small differences in the barriers and KIEs obtained from the different mechanisms in aqueous solution in the present study, and the fact that a more favorable entropy contribution is expected for the 6- and 8-membered ring TS mechanisms in the ribosome, this entropic term can be decisive to favoring these mechanisms.

■ ASSOCIATED CONTENT

ⓢ Supporting Information

Cartesian coordinates of QM atoms of TS-4, TS-6, and TS-8 located at M06-2X/MM level. This material is available free of charge via the Internet at http://pubs.acs.org.

■ AUTHOR INFORMATION

Corresponding Author

*moliner@uji.es; tunon@uv.es

Notes

The authors declare no competing financial interest.

■ ACKNOWLEDGMENTS

■ REFERENCES

(1) Yonath, A. *Angew. Chem., Int. Ed.* **2010**, *49*, 4341.
(2) Ramakrishnan, V. *Angew. Chem., Int. Ed.* **2010**, *49*, 4367.
(3) Steitz, T. A. *Angew. Chem., Int. Ed.* **2010**, *49*, 4388.
(4) Trobo, S.; Åqvist, J. *Proc. Natl. Acad. Sci. U.S.A.* **2005**, *102*, 12395.
(5) Trobo, S.; Åqvist, J. *Biochemistry* **2008**, *47*, 4898.
(6) Wallin, G.; Åqvist, J. *Proc. Natl. Acad. Sci. U.S.A.* **2010**, *107*, 1888.
(7) Jencks, W. P.; Blackburn, G. M. *J. Am. Chem. Soc.* **1968**, *90*, 2638.
(8) Satterthwait, A. C.; Jencks, W. P. *J. Am. Chem. Soc.* **1974**, *96*, 7018.
(9) Jencks, W. P. *Acc. Chem. Res.* **1976**, *9*, 425.
(10) Gresser, M. P.; Jencks, W. P. *J. Am. Chem. Soc.* **1977**, *99*, 6970.
(11) Cox, M. M.; Jencks, W. P. *J. Am. Chem. Soc.* **1981**, *103*, 572.
(12) Yang, C. C.; Jencks, W. P. *J. Am. Chem. Soc.* **1988**, *110*, 2972.
(13) Sawyer, C. B.; Kirsch, J. F. *J. Am. Chem. Soc.* **1973**, *95*, 7375.
(14) Bilkadi, Z.; de Lorimier, R.; Kirsch, J. F. *J. Am. Chem. Soc.* **1975**, *95*, 4317.
(15) Marlier, J. F.; Haptonstall, B. A.; Johnson, A. J.; Sacksteder, K. A. *J. Am. Chem. Soc.* **1997**, *119*, 8838.
(16) Marlier, J. F. *Acc. Chem. Res.* **2001**, *34*, 283.
(17) Seila, A. C.; Okuda, K.; Núñez, S.; Seila, A. F.; Strobel, S. A. *Biochemistry* **2005**, *44*, 4018.
(18) Hiller, D. A.; Zhong, M.; Singh, V.; Strobel, S. A. *Biochemistry* **2010**, *49*, 3868.
(19) Leung, E. K. Y.; Suslov, N.; Tuttle, N.; Sengupta, R.; Piccirilli, J. A. *Annu. Rev. Biochem.* **2011**, *80*, 527.
(20) Ilieva, S.; Galabov, B.; Musaev, D. G.; Morokuma, K.; Schaefer, H. F., III. *J. Org. Chem.* **2003**, *68*, 1496.
(21) Ilieva, S.; Galabov, B.; Musaev, D. G.; Morokuma, K. *J. Org. Chem.* **2003**, *68*, 3406.
(22) Galabov, B.; Atanasov, Y.; Ilieva, S.; Schaefer, H. F., III. *J. Phys. Chem. A* **2005**, *109*, 11470.
(23) Galabov, B.; Ilieva, S.; Hadjieva, B.; Atanasov, Y.; Schaefer, H. F., III. *J. Phys. Chem. A* **2008**, *112*, 6700.
(24) Chalmet, S.; Harb, W.; Ruiz-López, M. F. *J. Phys. Chem. A* **2001**, *105*, 11574.
(25) Singleton, D. A.; Merrigan, S. R. *J. Am. Chem. Soc.* **2000**, *122*, 11035.
(26) Sung, D. D.; Koo, I. S.; Yang, K.; Lee, I. *Chem. Phys. Lett.* **2006**, *426*, 280.
(27) Marenich, A. V.; Cramer, C. J.; Truhlar, D. G. *J. Phys. Chem. B* **2009**, *113*, 6378.
(28) Acosta-Silva, C.; Bertran, J.; Branchadell, V.; Oliva, A. *J. Am. Chem. Soc.* **2012**, *134*, 5817.
(29) Sÿtrajbl, M.; Florián, J.; Warshel, A. *J. Am. Chem. Soc.* **2000**, *122*, 5354.

(30) Oie, T.; Loew, G. H.; Burt, S. K.; Binkley, J. S.; MacElroy, R. D. *J. Am. Chem. Soc.* **1982**, *104*, 6169.

(31) Jensen, J. H.; Baldridge, K. K.; Gordon, M. S. *J. Phys. Chem. Soc.* **1992**, *96*, 8340.

(32) Yang, W.; Drueckhammer, D. G. *Org. Lett.* **2000**, *2*, 4133.

(33) Xia, X.; Zhang, C.; Xue, Y.; Kim, C. K.; Yan, G. *J. Chem. Theory Comput.* **2008**, *4*, 1643.

(34) Sharma, P. K.; Xiang, Y.; Kato, M.; Warshel, A. *Biochemistry* **2005**, *44*, 11307.

(35) Rangelov, M. A.; Vayssilov, G. N.; Yomtova, V. M.; Petkov, D. D. *J. Am. Chem. Soc.* **2006**, *128*, 4964.

(36) Bayryamov, S. G.; Rangelov, M. A.; Mladjova, A. P.; Yomtova, V. M.; Petkov, D. D. *J. Am. Chem. Soc.* **2007**, *129*, 5790.

(37) Rangelov, M. A.; Petrova, G. P.; Yomtova, V. M.; Vayssilov, G. N. *J. Org. Chem.* **2010**, *75*, 6782.

(38) Świderek, K.; Tuñón, I.; Martí, S.; Moliner, V.; Bertran, J. *Chem. Commun.* **2012**, *48*, 11253.

(39) Dewar, M. J. S.; Zoebisch, E. G.; Healy, E. F.; Stewart, J. J. P. *J. Am. Chem. Soc.* **1985**, *107*, 3902.

(40) Zhao, Y.; Truhlar, D. G. *Theor. Chem. Acc.* **2008**, *120*, 215.

(41) Zhao, Y.; Truhlar, D. G. *Acc. Chem. Res.* **2008**, *41*, 157.

(42) Jorgensen, W. L.; Chandrasekhar, J.; Madura, J. D.; Impey, R. W.; Klein, M. L. *J. Chem. Phys.* **1983**, *79*, 926.

(43) Field, M. J.; Albe, M.; Bret, C.; Proust-De Martin, F.; Thomas, A. *J. Comput. Chem.* **2000**, *21*, 1088.

(44) Turner, A. J.; Moliner, V.; Williams, I. H. *Phys. Chem. Chem. Phys.* **1999**, *1*, 1323.

(45) Martí, S.; Moliner, V.; Tuñón, I. *J. Chem. Theory Comput.* **2005**, *1*, 1008.

(46) Kumar, S.; Bouzida, D.; Swendsen, R. H.; Kollman, P. A.; Rosenberg, J. M. *J. Comput. Chem.* **1992**, *13*, 1011.

(47) Torrie, G. M.; Valleau, J. P. *J. Comput. Phys.* **1977**, *23*, 187.

(48) Verlet, L. *Phys. Rev.* **1967**, *159*, 98.

(49) Stern, M. J.; van Hook, W. A.; Wolfsberg, M. *J. Chem. Phys.* **1963**, *39*, 3179.

(50) Martí, S.; Moliner, V.; Tuñón, I.; Williams, I. H. *J. Phys. Chem. B* **2005**, *109*, 3707.

(51) Martí, S.; Moliner, V.; Tuñón, I.; Williams, I. H. *Org. Biomol. Chem.* **2003**, *1*, 483.

(52) Ruggiero, G. D; Guy, S. J.; Martí, S.; Moliner, V.; Williams, I. H. *J. Phys. Org. Chem.* **2004**, *17*, 592.

(53) Schroeder, G. K.; Wolfenden, R. *Biochemistry* **2007**, *46*, 4037.

(54) Pu, J.; Ma, S.; Garcia-Viloca, M.; Gao, J.; Truhlar, D. G.; Kohen, A. *J. Am. Chem. Soc.* **2005**, *127*, 14879.

(55) Kolmodin, K.; Luzhkov, V. B.; Åqvist, J. *J. Am. Chem. Soc.* **2002**, *124*, 10130.

(56) Hengge, A. C.; Hess, R. A. *J. Am. Chem. Soc.* **1994**, *116*, 11256.

(57) O'Leary, M. H.; Marlier, J. F. *J. Am. Chem. Soc.* **1979**, *101*, 3300.

(58) Sawyer, C. B.; Kirsch, J. F. *J. Am. Chem. Soc.* **1973**, *95*, 7375.

(59) Kingery, D. A.; Strobel, S. A. *Acc. Chem. Res.* **2012**, *45*, 495.

(60) Hiller, D. A.; Singh, V.; Zhong, M.; Strobel, S. A. *Nature* **2011**, *476*, 236.

(61) Kaminski, Z. J.; Paneth, P.; O'Leary, M. H. *J. Org. Chem.* **1991**, *56*, 5716.

(62) Sievers, A.; Beringer, M.; Rodnina, M. V.; Wolfenden, R. *Proc. Natl. Acad. Sci. U.S.A* **2004**, *101*, 7897.

(63) Beringer, M.; Bruell, C.; Xiong, L.; Pfister, P.; Bieling, P.; Katunin, V. I.; Mankin, A. S.; Böttger, E. C.; Rodnina, M. V. *J. Biol. Chem.* **2005**, *280*, 36065.